Detent Force Analysis and Optimization for Vertical Permanent-magnet Linear Synchronous Motor with Fractional-slot Windings

Xiaozhuo Xu
School of Electrical Engineering and Automation, Henan Polytechnic University, Jiaozuo, P.R. China
Email: xxz@hpu.edu.cn

Xudong Wang, Jikai Si, Haichao Feng and Baoyu Xu
School of Electrical Engineering and Automation, Henan Polytechnic University, Jiaozuo, P.R. China
Email: {wangxd, sijikai, fhc, xubaoyu}@hpu.edu.cn

***Abstract*—This paper investigates the detent force modeling and optimization of a iron-core type 16-pole 15-slot permanent magnet linear synchronous motor (PMLSM) for ropeless elevator applications. Variable network non-linear magnetic equivalent circuit (VNMEC) model is established to predict the detent force of PMLSM. The topology structure of equivalent magnetic circuit is developed and the permeance are derived and calculated. The end effect of two end teeth is essential for detent force analysis and it is focused in the modeling. Magnetic saturation of primary tooth also is taken into account and nonlinear permanence is calculated. Some 3-D finite-element numerical calculations are used to validate the feasibility of the proposed method. Then proposed VNMEC is employed to calculate and optimize the detent force considering the end tooth dimensions. In final, experimental results are further used to verify the validation of proposed model.**

***Index Terms*—permanent-magnet linear synchronous motor, 16-pole 15-slot structure, detent force, equivalent magnetic network, optimization design**

I. INTRODUCTION

Recently, following the increasing height of the buildings and depth of mines, the traditional rope hoist system such as elevator and mine hoist is limited in lifting height and speed and effective weight due to the ropes exist. It is urgent to develop a new hoist mode instead of the traditional ones. The vertical hoist system driven by linear motor is of potential best choice to solve the hoisting problems for the high-rise buildings and ultra-deep mine [1-4]. And it attracts much more attentions because of its many advantages such as large thrust density, high efficiency, fast response, accurate positioning, simple structure and no height limit and so on[5-6].

In comparison with linear switched reluctance motor (LSRM) and linear induction motor (LIM), the permanent magnet linear synchronous motor (PMLSM) is most suitable drive source for vertical hoist system because of the high force density. Especially, the slotted iron core PMLSM with fractional-slot concentrated windings has larger force density and shorter end windings than that with distribution windings, and more suitable for long stroke ropeless hoist applications [7]. However, PMLSM with primary core opening slots and both breaking ends has the detent force caused by the cogging effect and end effect, which will lead to thrust fluctuations, affecting the low-speed performance and positioning accuracy. Therefore, prediction and reduction of detent force are highly important research aspects in permanent magnet linear motor [8-10]. Currently, there are mainly three ways to calculate the detent force of PMLSM, i.e., numerical method [8], analytical method, and magnetic equivalent circuits. Numerical method mainly refers to the finite-element method, which is accurate and suitable for evaluating final designs, but is computationally complexity and time consuming in pre- and post-processing, especially in the stage of optimization design which often changes the motor structure parameters. The analytical method mainly uses layer linear models to analyze the fundamental and harmonic components of detent force quickly by means of Fourier series [9-10], however, many simplifications are done in physical models like ignoring detail structure, magnetic saturation and magnetic flux leakage of permanent magnet, and this decreases the accuracy of results. Magnetic equivalent circuits can provide a compromise between finite element and analytical method, which has higher accuracy than analytical method and far less computation time than the finite element method. Currently, this method has been used to calculate the air-gap magnetic field, back-EMF and other cases [11-12], but rarely used to investigate the detent force of PMLSM.

In addition, researchers have proposed some detent force reduction techniques such as using stair shape auxiliary teeth, skewing PM poles or slots, optimizing iron-core length, but some of them affect machine output or driving characteristics [13]. The detent force in slotted iron-core PMLSM is composed of the end component and the cogging component. Generally, the former is much larger than the latter. Recently, fractional-slot

doi:10.4304/jcp.8.3.756-763

concentrated windings is adopted in PMLSM[14-16], greatly reduces the slot cogging force and remains large force density, but the end component of detent force still exists and dominates the major part. In [17], the end tooth length is optimized to reduce the detent force using general magnetic circuit analytical model ignored the iron-core saturation effect.

In this paper, the targets are to predict and reduce the detent force of 16-pole 15-slot structure PMLSM. A simplified nonlinear magnetic equivalent network model is established considering the structural characteristics of PMLSM. Tooth tip local saturated permeance is calculated according to the magnetization curve of the iron-core considering the local saturation. Two end teeth of the iron-core are focused in modeling process and their optimal length and width are also calculated and discussed. The results are verified by three-dimensional finite element calculations and experiments.

II. Ropeless Elevator and Linear Motor Model

A. Ropeless Elevator Driven by PMLSM

The ropeless elevator system as the main future vertical transportation mode is of breakthrough the limitation of the buildings height. Two types linear motor elevator developed by author's group are shown in Fig.1.

(a)double-sided stator (b) single-sided stator

Figure 1. Ropeless hoist system driven by PMLSM.

The left one with vertical travel 3 meters and effective load 20 Kg, is composed of two double-side PMLSM stator with distribution windings and permanent magnet mover. The right one is called home ropeless elevator with vertical travel 4 meters and rated load 2 adults, composed of single-side PMLSM stator with fractional-slot concentrated windings and permanent magnet mover. The 16-pole 15-slot PMLSM has larger thrust-volume-ratio than other pole-slot combinations and so it is chosen as the standard unit motor with 15slots length. Meanwhile, the caliper brake with the force amplifier was designed and developed independently in ropeless elevator applications and it has smaller size and larger braking force, operating faster and more reliably than the existing ordinary brake. In addition, the home ropeless elevator has four security protections such as working caliper brake, safety gear over-speed protection and bottom buffer protection, and especially employing specific power failure emergency protection due to the inherent character of PMLSM that the primary windings are shorted automatically when power failure occurs and then moving secondary permanent magnets cut the closed coils and the brake force is generated by Lenz's law.

B. PMLSM with Fractional-slot Concentrated Windings

Considering the practical application of vertical ropeless hoist system, such as suitable unit motor weight, maximum thrust-volume ratio, economical metal materials and easy installation, fractional-slot concentrated windings PMLSM is selected as the driving motor of ropeless elevator.

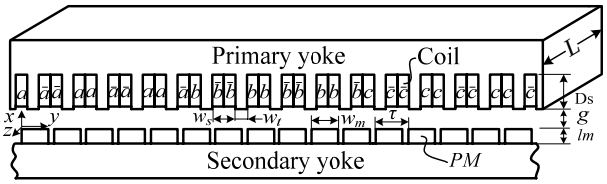

Figure 2. Model of 16-pole 15-slot iron-core PMLSM.

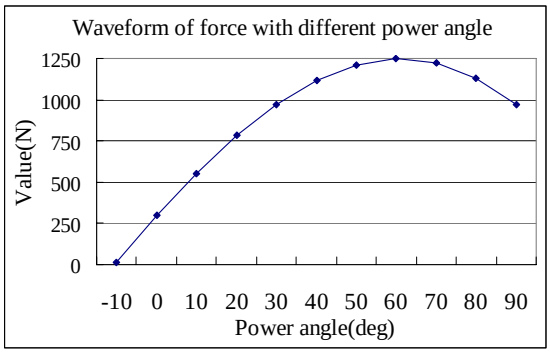

Figure 3. Waveform of thrust with different power angle.

TABLE I.

SPECIFICATION OF PMLSM

Items[units]	value	Items[units]	value
Iron-core length[mm]	336	Number of slot	15
Limitation thickness[mm]	100	PM height[mm]	9
Slot width[mm]	14	PM width[mm]	18
Tooth height[mm]	20	Pole pitch[mm]	21
Tooth width[mm]	8.4	Air-gap[mm]	2.6

Fig.2 shows the main physical structure and winding configuration. Table I shows the main parameters of fractional-slot concentrated windings PMLSM. Fig.3 shows the characteristic of thrust vs. power angle in steady status. This motor has two prominent advantages that having small cogging torque due to fractional-slot

iron-core structure, and having high winding factor and low loss and saving metal martial due to adopting primary concentrated windings which has more shorter end than distribution windings.

III. Detent Force Modelling

A. Variable Network Magnetic Equivalent Circuit Model

Variable network magnetic equivalent circuit model (VNMEC) is discussed in this section. Fig.4 shows the open-circuit field distribution. Fig.5 shows the magnetic equivalent circuit model of the whole motor. During the movement of mover, the magnetic network changes when all the permeance changes with the distance Δx shown in Fig.5, therefore, it is a variable network equivalent magnetic circuit model.

The VNMEC model consists of the equivalent permeance of the primary and secondary, the air-gap permeance and edge permeance. The symbols in Fig. 5 are explained as follows. F_m is magnetic motive force (MMF); G_{ma} , G_{mb} , G_{mc} are magnet inner permeance; G_{ys} is secondary yoke permeance; G_{PML} is permeance caused by the self leakage flux of a PM pole; G_{PMM} is permeance caused by adjacent magnets leakage flux; G_n is air-gap permeance; G_L is leakage permeance between adjacent teeth; G_{L3D} is 3-D leakage permeance in the end region of motor; G_t is primary middle tooth permeance; G_{te} is primary end tooth permeance; G_{tp} is primary middle permeance tip; G_{tpe} is primary end tip permeance; G_y is primary yoke presence.

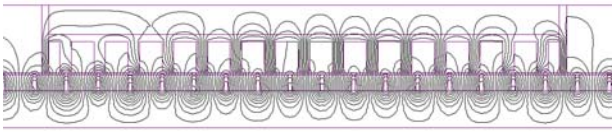

Figure 4. Flux distribution of 16-pole 15-slot PMLSM.

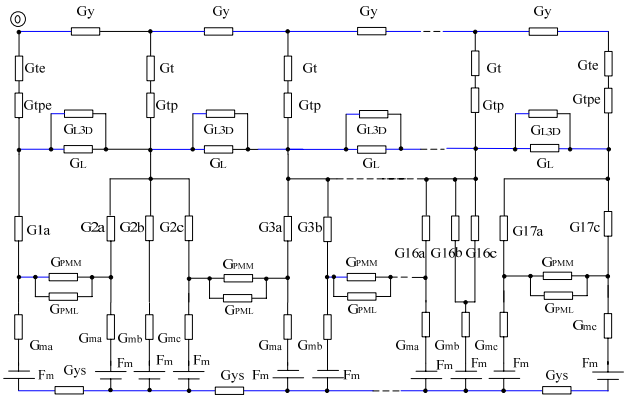

Figure 5. Equivalent magnetic model of 16-pole 15-slot PMLSM.

B. Air-gap Permeance Calculation

To simplify the calculation of air-gap permeance, we assumed that the surfaces of the stator and rotor core are magnetic equipotent surface respectively. The magnetic flux lines are vertical to the surface of the core. The flux paths at the boundary flowing to adjacent teeth are moving in the same length [18].

According to different relative positions of the stator and mover, the air-gap permeance are obtained based on magnetic flux tubes with boundaries determined by straight line and semicircular segments instead of the actual magnetic flux lines. The main schematic diagrams are shown as Fig.6.

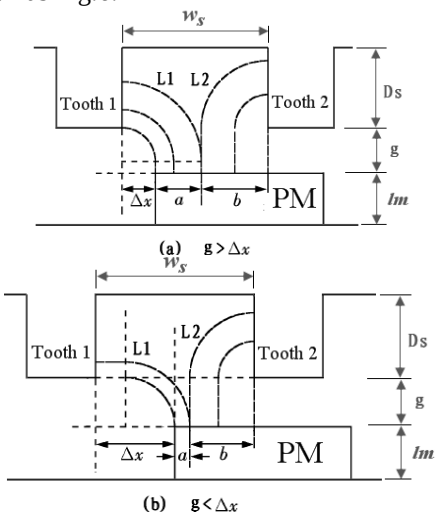

Figure 6. Flux path of one stator segment for different rotor positions.

When the relative position of the PM and the tooth is shown in Fig.4(a), that is $g > \Delta x$, the average length flowing to tooth 1 and tooth 2 L_a and L_b are given by

$$L_a = g - \Delta x + \frac{\pi}{2}(\Delta x + \frac{a}{2}), \quad L_b = g + \frac{\pi}{4}b \tag{1}$$

where

$$a = \frac{w_s}{2} - \Delta x + \frac{\Delta x}{\pi}, \quad b = \frac{w_s}{2} - \frac{\Delta x}{\pi} \tag{2}$$

The corresponding permeance are given by

$$G_a = \frac{\mu_0 a L}{L_a} = \frac{\mu_0 L(\frac{w_s}{2} - \Delta x + \frac{\Delta x}{\pi})}{g - \frac{3}{4}\Delta x(\pi - 1) + \frac{\pi}{8}w_s} \tag{3}$$

$$G_b = \frac{\mu_0 b L}{L_b} = \frac{\mu_0 L(\frac{w_s}{2} - \frac{\Delta x}{\pi})}{g - \frac{1}{4}\Delta x + \frac{\pi}{8}w_s} \tag{4}$$

When the relative position of the PM and the tooth is shown in Fig.4(b), that is $g < \Delta x$, the average length flowing to tooth 1 and tooth 2 L_a and L_b are given by

$$L_a = g - \Delta x + \frac{\pi}{2}(g + \frac{a}{2}), L_b = g + \frac{\pi}{4}b \tag{5}$$

where

$$\begin{cases} a = \frac{w_s}{2} - \frac{\Delta x}{2} - \frac{\Delta x}{\pi} + \frac{2g}{\pi} - \frac{g}{2} \\ b = \frac{w_s}{2} - \frac{\Delta x}{2} + \frac{\Delta x}{\pi} - \frac{2g}{\pi} + \frac{g}{2} \end{cases} \quad (6)$$

The corresponding permeance are given by

$$G_a = \frac{\mu_0 a L}{L_a} = \frac{\mu_0 L(\frac{w_s}{2} - \frac{\Delta x}{2} - \frac{\Delta x}{\pi} + \frac{2g}{\pi} - \frac{g}{2})}{\frac{3}{4}\Delta x - \frac{1}{2}g - \frac{\pi}{4}(\frac{1}{2}w_s - \frac{1}{2}\Delta x + \frac{3g}{2})} \quad (7)$$

$$G_b = \frac{\mu_0 b L}{L_b} = \frac{\mu_0 L(\frac{w_s}{2} - \frac{\Delta x}{2} + \frac{\Delta x}{\pi} - \frac{2g}{\pi} + \frac{g}{2})}{\frac{g}{2} + \frac{\pi}{4}(\frac{w_s}{2} - \frac{\Delta x}{2} + \frac{\Delta x}{\pi} + \frac{g}{2})} \quad (8)$$

The air gap permeance includes two parts. The permeance taking into account the cross-section area of the mover and the stator can be calculated using air-gap length by geometric methods. The average permeance modeling the flux paths which flow from the stator PM to two sides of mover teeth is calculated by (3), (4), (7) and (8). Then the air-gap permeance corresponding to different branches can be obtained through adding two parts together.

C. The Primary Equivalent Permeance

The primary equivalent permeance consists of yoke permeance G_y, tooth permeance G_t and G_{tp} and leakage permeance between adjacent teeth G_L. In order to consider the local magnetic saturation in the tooth, the tooth tip permeance G_{tp} is provided within a certain distance from the tooth tip (near the air gap side) considering the magnetic saturation effect, composed of G_{br}, G_{tr}, G_{bl}, G_{tl} and G_{ta} discussed later.

Tooth permeance G_t and leakage permeance between adjacent teeth G_L are given by

$$G_t = \frac{\mu_0 \mu_{Fe} w_t L}{D_s(1-\alpha)}, \; G_L = \frac{\mu_0 D_s L}{2 w_s} \quad (9)$$

Meanwhile, the leakage permeance G_{L3D} is expressed by

$$G_{L3D} = 2\mu_0 (w_t - \frac{w_s}{2})\left[0.268 + 0.318 \ln(1 + \frac{w_t}{w_s})\right] \quad (10)$$

D. The Secondary Equivalent Permeance

The MMF source produced by the permanent magnets in secondary can be represented as $F_m = \frac{B_m H_m}{\mu_m}$, where H_m, B_m, μ_m are the magnet thickness, the magnetic density and magnet permeability, respectively. The leakage permeance G_{PMM} and G_{PML} are given by

$$\begin{cases} G_m = \frac{\mu_0 \mu_{rm} w_m L}{D_s}, G_{PML} = \frac{\mu_0 L(\tau - w_m)}{l_m} \\ G_{PMM} = \frac{2\mu_0 L}{\pi} \ln(1 + \frac{g\pi}{\tau - w_m}) \end{cases} \quad (11)$$

E. Saturation Effect in Stator Tooth

Fig. 6 shows the local magnetic field distribution when the stator and mover poles are partly overlapping. In Fig. 6(a), the heavy line represents the leakage flux path. The flux loops are short circuited via the pointed end of the stator tooth. In order to capture the local magnetic saturation, an analytical model of air-gap permeance is presented and shown in Fig. 6(b). G_{br}, G_{tr}, G_{bl}, G_{tl} and G_{ta} are saturation permeance tips in the stator tooth and are given by

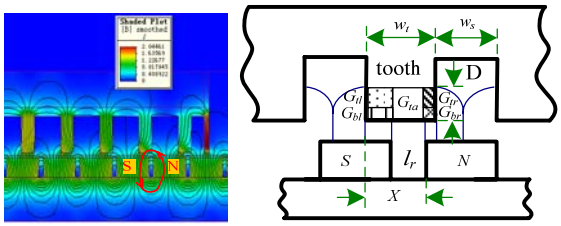

(a) (b)

Figure 7. Magnetic field distribution with a stator tooth aligns with magnet pole spacer.

$$\begin{cases} G_{br} = \frac{2\mu_0 \mu_{br} k_i L(X - w_s)}{D}, G_{tr} = \frac{2\mu_0 \mu_{tr} k_i L(X - w_s)}{D} \\ G_{bl} = \frac{2\mu_0 \mu_{bl} k_i L(\frac{w_s}{2} + w_t - X)}{D}, G_{tl} = \frac{2\mu_0 \mu_{tl} k_i L(\frac{w_s}{2} + w_t - X)}{D} \\ G_{ta} = \frac{\mu_0 \mu_{ta} k_i L D}{l_r} \end{cases} \quad (12)$$

where $D = \min(T_s - X, X - l_r)$.

IV. Detent Force Prediction and Optimization

A. Equivalent Network Equations

In Fig.5, the number of branches of the equivalent magnetic circuits varies with mover position while the number of nodes in the circuit is fixed. So the nodal analysis is used to solve the magnetic circuit. The magnetomotive source due to the magnets can be represented by two possible magnetic branches as shown in Fig.6, in which k_{i1} and k_{i2} represent the nodes connected by branch i, $F_m(k_{i1})$ and $F_m(k_{i2})$ are the magnetic potential, $\phi(i)$ is the flux through branch i, $G_m(i)$ is the branch permeance, $F_{m0}(i)$ is the branch magnetomotive source, and $\phi_0(i)$ is the branch magnetic flux source. These parameters have the following relationship:

$$\begin{cases} \phi(i) = P_m(i)[F_m(k_{i1}) - F_m(k_{i2})] + \phi_0(i) \\ \phi_0(i) = P_m(i) F_{m0}(i) \end{cases} \quad (13)$$

$$\begin{bmatrix} G(1,1) & G(1,2) & \cdots & G(1,m) \\ G(2,1) & G(2,2) & \cdots & G(2,m) \\ \vdots & \vdots & \vdots & \vdots \\ G(m,1) & G(m,2) & \cdots & G(m,m) \end{bmatrix} \begin{bmatrix} F_m(1) \\ F_m(2) \\ \vdots \\ F_m(m) \end{bmatrix} = \begin{bmatrix} \phi_s(1) \\ \phi_s(2) \\ \vdots \\ \phi_s(m) \end{bmatrix} \quad (14)$$

where m is number of independent nodes; $G(i, j)$, for i, $j=1,2,\ldots m$, is the node permeance; $F_m(i)$, for $i=1,2,\ldots m$,

is the node magnetic vector potential; $\phi_m(i)$, for $i=1,2,\ldots m$, is the node magnetic flux source.

In short form, it can be written as

$$G_m(\mu_i)F_m = \phi_s(\mu_i) \tag{15}$$

where μ_i is permeability of branch i; $G_m(\mu_i)$ is node permeance matrix; F_m is vector of node magnetic potential; $\phi_s(\mu_i)$ is vector of node magnetic flux source.

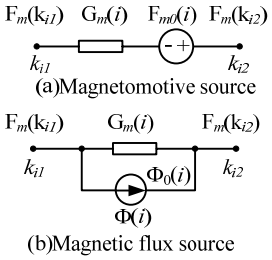

Figure 8. representation of possible magnetic branches.

Gauss-Seidel iteration method is employed to solve (5), nonlinear iterative process is shown as follow.

$$G(\mu_i)^{(k)} F_m^{(k)} = \phi_s(\mu_i)^{(k)} \tag{16}$$

Where, $G(\mu_i)$ is composed of air-gap permeance, leakage permeance and iron-core permeance. Air-gap permeance and leakage permeance is linear and can be calculated directly when mover has a displacement Δx . Iron-core nonlinear permeance $G_m(\mu_i)$ is iterated through B-H curve of iron-core material as follow.

$$G_n(\mu_i)^{(k)} = \mu_i^{(k)} \frac{S_m}{L_m} \tag{17}$$

$$\mu_i^{(k)} = \frac{B_i^{(k-1)}}{H_i^{(k-1)}} \tag{18}$$

B. Magnetic Field and Detent Force Prediction

The magnetic energy storage for each branch is given by

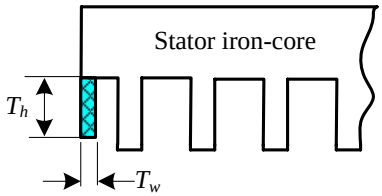

Figure 11. End tooth configuration (side view).

$$W_{mi} = \frac{1}{2} F_{mi} \Phi_{fi} \tag{19}$$

The total magnetic energy storage can be expressed as follows.

$$W_{MA} = \sum W_{mi} = \sum \frac{1}{2} F_{mi} \Phi_{fi} = \sum \frac{1}{2} F_{mi}(G_i F_{mi}) = \frac{1}{2} \sum (F_{mi}^2 G_i) \tag{20}$$

The detent force produced by PMLSM is given by

$$F_{cog} = \frac{\partial W_{MA}}{\partial x} \tag{21}$$

When the mover position is changed, the permeance of each branch should be recalculated again, and then the detent force of mover can be obtained in every position. Fig.9 and Fig.10 show the calculated curves about the air-gap flux density distribution and the detent force with the mover position. The proposed method is validated by the 3-D finite element analysis (FEA).

Fig.9 shows the comparison of the calculated detent force by VNEMC and 3-D FEA results within a pole pitch. From this figure, the maximum error is calculated at 9.8%. This method basically meets the engineering needs and the calculated speed are greatly increased, the computing time reduced to 55seconds, while the time of three-dimensional FEA is up to 8 hours. Proposed method provides a way to design optimization of PMLSM quickly.

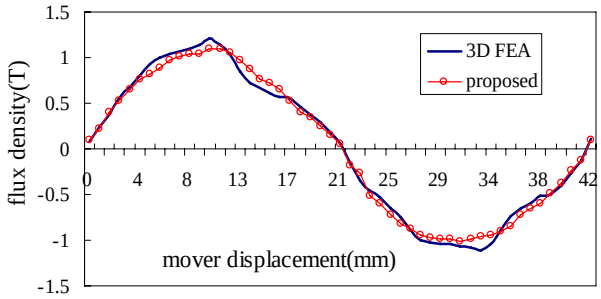

Figure 9. Flux distribution of 16-pole 15-slot PMLSM.

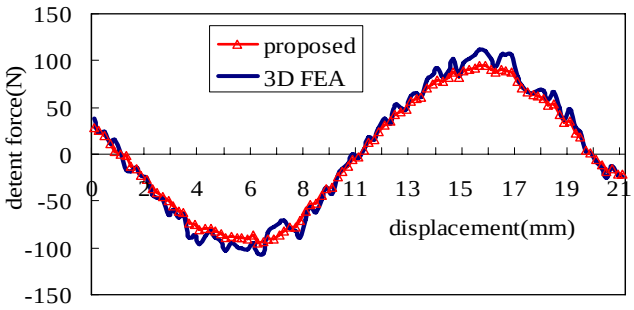

Figure 10. Flux distribution of 16-pole 15-slot PMLSM.

C. Detent Force Optimization

The finite length of the armature core results in a detent force [19]. Two end teeth of PMLSM have obviously contributions to the detent force fluctuating with pole pitch periodically. Optimizing the end tooth dimensions, can be used to reduce the detent force.

We analyzed the detent force of the basic model with two edge end teeth using the proposed VNEMC method by adjusting the tooth heights and widths. Fig.11 shows the end tooth configuration (side view).

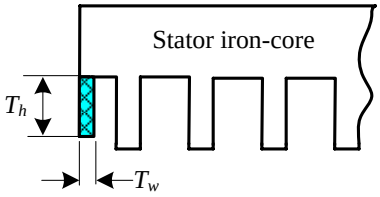

Figure 11. End tooth configuration (side view).

Fig.12 shows detent force characteristics comparison with different end tooth heights by proposed VNEMC at the 2.6-mm air gap. From Fig.13, it can be summarized

that the end tooth heights extremely influence the detent magnitude, when the height is smaller than 13*mm*, equal to the air-gap is longer than 7*mm*, the detent force is reduced by 70% than full height and almost less affected by end tooth height.

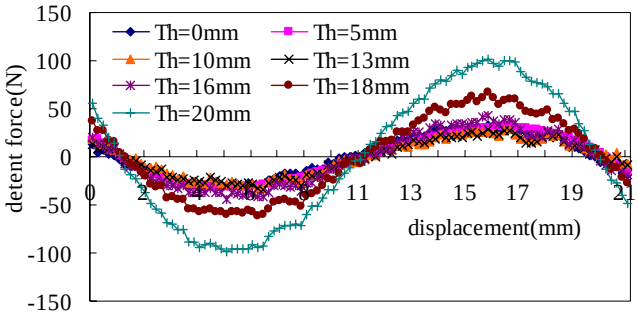

Figure 12. detent force comparison by different end tooth height.

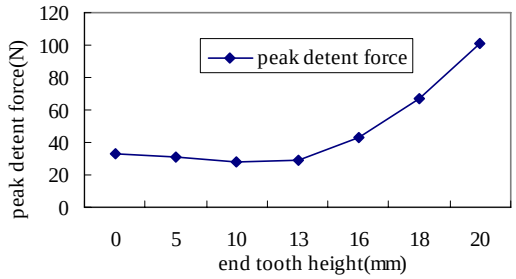

Figure 13. Trend of detent force with tooth height variation.

Meanwhile, with a constant air-gap 2.6*mm*, varying the end tooth widths, detent force characteristics are shown in Fig.14 and Fig.15. We can see that there is tooth width (=15*mm*) producing a minimal detent force magnitude (=21N). When end tooth width is smaller than 4 *mm* or bigger than 18 *mm*, detent force increases significantly.

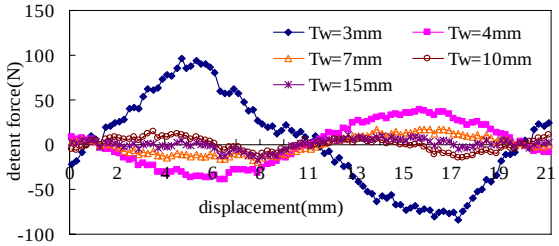

Figure 14. Detent force comparison by different end tooth width.

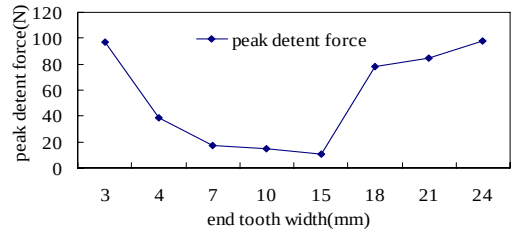

Figure 15. Trend of detent force with tooth width variation.

V. MEASUREMENTS

A. Laboratory Prototype and Set-up

The studied laboratory prototype is shown in Fig.16. The parameters used for the active parts of the machine are given in Table I. The experiment setup is equipped with test motor, drive motor and its driver and force senor are shown in Fig.17. In this paper, we use two test motors that one has end teeth and another has no end tooth. The mover displacement is also measured by using linear encoders. When do the tests, firstly, remove the test motor and remain the drive motor has a constant velocity to run, and then we can test the frictional force of the whole mover system. Then add the test motor to the experiment bench and record the thrust force data. The net detent force is the thrust force minus the frictional force.

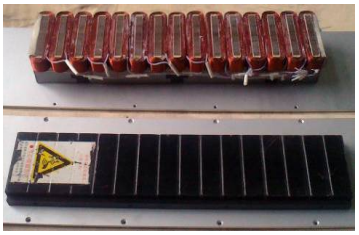

Figure 16. Experimental 16pole-15slot motor.

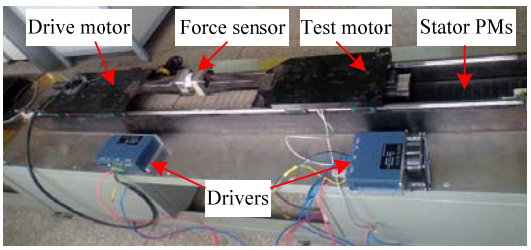

Figure 17. experiment setup.

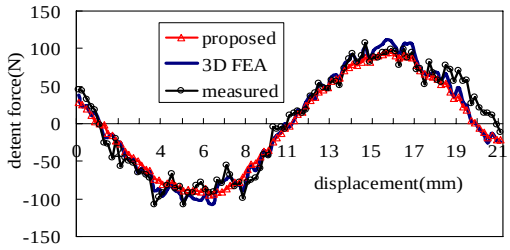

Figure 18. Detent force curve with end tooth Th=20mm,Tw=4mm.

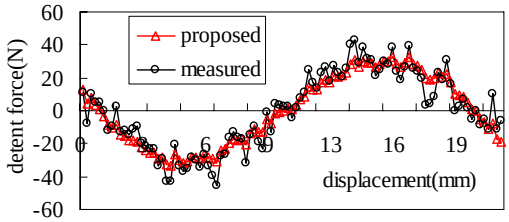

Figure 19. Detent force curve with no end tooth

B. Experimental Results

The measured detent force with end tooth ($T_h = 20mm, T_w = 4mm$) is shown in Fig.18. After the optimal design of the edge tooth dimensions, another motor prototype with no end tooth are test and the data are shown in Fig.19. From Fig.18 and Fig.19, we can see that the experiment results well agree with the proposed results.

VI. CONCLUSIONS

This paper studies the detent force modeling and optimization of PMLSM using for ropeless elevator and establishes the variable network non-linear magnetic equivalent circuit model of PMLSM. The end effect of two end teeth and magnetic saturation of primary iron-core are taken into account in the modeling. 3-D finite-element analysis and experiment measured data is employed to evaluate the proposed method. It shows that the proposed method can solve the problem effectively without much time consuming, could be used to study the PMLSM characteristics and optimal design of ropeless elevator.

ACKNOWLEDGMENT

The work was possible due to the support given by the National Science Foundation of China (61074095), Research Fund for the Doctoral Program of Higher Education (20104116120001), Innovation Project for University Prominent Research Talents (2005126), Natural Science Program of Henan province (2011A470003), Research Projects of China National Coal Association (MTKJ2011-397) and Key Lab of Precision manufacturing technology and engineering (PMTE201010A), especially the Innovation Talents Foundation of Henan Province (104200510021) to the authors.

REFERENCES

[1] Cagri Gurbuz, Ender Kazan, Ahmet Onat, Sandor Marko, "Linear motor for multi-car elevators: Design and position measurement", *Turkish Journal of Electrical Engineering and Computer Sciences*, vol.19, pp. 827-838, 2011.

[2] Xudong Wang, Haichao Feng, Baoyu Xu, Xiaozhuo Xu, "Research on rope-less hoist system driven by PMLSM", Advanced Materials Research, vol.216, pp. 539-543, June 2011.

[3] Y.W. Zhu, D.S. Kim, D.H. Kooa, Y.H. Cho, "Optimal design of a double-sided slotted iron core type PMLSM with manufacturing considerations", *Applied Electromagnetic Engineering: Magnetic Superconducting and Nano Materials*, vol.670, pp. 235-242, June 2011.

[4] Ahmet Onat, Ender Kazan, Norio Takahashi, Daisuke Miyagi, Yasuhiro Komatsu, Sandor Markon, "Design and implementation of a linear motor for multicar elevators", *IEEE/ASME Transactions on Mechatronics*, vol.15, pp. 685-693, October 2010.

[5] Tetsuzo Sakamoto, Toyokazu Hanamoto, "Modeling and robust control system design of a ropeless elevator driven by LSM", *IEEJ Transactions on Industry Applications*, vol.130, pp. 760-767+7, 2010.

[6] Xiaozhuo Xu, Xudong Wang, Shiying Yuan and Haichao Feng, "Optimization of vertical linear synchronous motor for ropeless elevator with INGA method", *International Conference on Electrical and Control Engineering*, vol.1, pp.3965-3968, June 2010.

[7] Yu-wu Zhu, Sang-geon Lee and Yun-hyun Cho, "Topology structure selection of permanent magnet linear synchronous motor for ropeless elevator system", *IEEE International Symposium on Industrial Electronics (ISIE)*, pp.1523-1528, July 2010.

[8] Gabriele Gilardi, Kei Szeto, Steve Huard, Edward J. Park, "Finite element analysis of the cogging force in the linear synchronous motor array for the Thirty Meter Telescope", *Mechatronics*, vol. 21, pp. 116-124, February 2011.

[9] Hao Wang, Zhijing Zhang, Chengying Liu, "Compensation methods of longitudinal end effects in permanent-magnet linear synchronous motor", *Proceedings of the Chinese Society of Electrical Engineering*, vol. 30, pp. 46-52, December 2010.

[10] Xuanfeng Shangguan, Shiying Yuan, Qingfu Li, "Study on cogging force of permanent magnet linear synchronous motor", *Journal of Coal Science and Engineering*, vol. 11, pp. 89-92, June 2005.

[11] Shi-Uk Chung, Ji-Won Kim, Byung-Chul Woo, Do-Kwan Hong, Ji-Young Lee, Dae-Hyun Koo, "Force ripple and magnetic unbalance reduction design for doubly salient permanent magnet linear synchronous motor", *IEEE Transactions on Magnetics*, vol. 47, pp. 4207-4210, October 2011.

[12] Ki-Bong Jang, Jee-Hyun Kim, Ho-Jin An, Gyu-Tak Kim, "Optimal design of auxiliary-teeth to solve circulation current reduction of permanent magnet linear synchronous motor", *Journal of Central South University of Technology*, vol. 18, pp. 690-696, June 2011.

[13] Yu Chen, Z.Q. Zhu, David Howe, "Three-dimensional lumped-parameter magnetic circuit analysis of single-phase flux-switching permanent-magnet motor", *IEEE Transactions on Industry Applications*, vol. 44, pp. 1701-1710, 2008.

[14] Wei Hua, Gan Zhang, Ming Cheng, Jianning Dong, "Electromagnetic performance analysis of hybrid-excited flux-switching machines by a nonlinear magnetic network model", *IEEE Transactions on Magnetics*, vol. 47, pp. 3216-3219, October 2011.

[15] Yoshiaki Kano, Takashi Kosaka, Nobuyuki Matsui, "A simple nonlinear magnetic analysis for axial-flux permanent-magnet machines", *IEEE Transactions on Industrial Electronics*, vol. 57, pp. 2124-2133, June 2010.

[16] Nyambayar Baatar, Hee Sung Yoon, Minh Trien Pham, Pan Seok Shin, Chang Seop Koh, "Shape optimal design of a 9-pole 10-slot PMLSM for detent force reduction using adaptive response surface method", *IEEE Transactions on Magnetics*, vol. 45, pp. 4562-4565, October 2009.

[17] Yong-Jae Kim, Sang-Yong Jung, "Minimization of outlet edge force using stair shape auxiliary teeth in a stationary discontinuous armature linear permanent magnet motor", *IEEE Transactions on Magnetics*, vol. 47, pp. 3228-3231, October 2011.

[18] C.Ming, C.C.Chan,etal, "Nonlinear Varying-Network Magnetic Circuit Analysis for Doubly Salient Perment-Magnet Motors". *IEEE Trans. on Magnetics*, Vol.36, pp.339-347, 2005.

[19] Sang-Min Jin, Yu-Wu Zhu, Sung-Hyung Lee, Yun-Hyun Cho, "Optimal design of auxiliary poles to minimize detent force of permanent magnet linear synchronous motor", *International Journal of Applied Electromagnetics and Mechanics*, vol.33, pp. 589-595, 2010.

Xiaozhuo Xu was born in Henan, P.R. China in 1980, and received the B.S. and M.S. degrees in electrical engineering and automation, Electrical machinery and appliances from School of Electrical Engineering and Automation, Henan Polytechnic University, P.R. China. His research interests are analysis of physical field

for special motor, optimization design of linear and rotary machines.

He is currently a doctoral candidate and engaged in the research on computer-aided optimum design of linear motors. From 2007 to 2008, he was a visiting research partner, supported by the ASM Pacific Technology Ltd., Hong Kong, and mainly focused in cogging force optimum of Direct Drive motors.

Xudong WANG was born in China in 1967, and received the PH.D degree in electrical engineering from School of Electrical engineering, Xi'an Jiaotong University, China, in 2002. From 2003 to 2004, he was carried out the postdoctoral research project in the University of Sheffield, UK, as a visiting scholar. His research interests are linear motor theory and control, motor optimization, design of linear motor driving system, energy efficient motors.

He is a Professor of electrical engineering and Vice-dean in School of Electrical Engineering and Automation, Henan Polytechnic University, china. As the Director of Institute of Linear Motor and Drive in Henan Polytechnic University, he achieved 30 research projects, including 4 the National Natural Science Foundation of China, and over 80 papers was published, among which over 20 was embodied by EI and SA. He has 13 national invention patents and 9 utility model authorization patents in China. He presided to develop many experimental system or products, such as rope-less hoist system with high-power, home elevator driven by PMLSM, automatic precision servo system, high temperatures superconducting Maglev vehicles, efficient asynchronous motor, self-starting PM motor, and so on. Now, he has 9 projects are being undertaken about multi-car rope-less hoist system driven by PMLSM.

Dr. WANG is the one of the academic technology leaders, key academic leader of key discipline of Motor and Electrical, Science and Technology Innovation outstanding talent in Henan Province, China. He is the member of the International Electromagnetic (ICS) and linear motor special committee of China.

Jikai SI was born in Henan Province, China, in 1973. He received the B.S. and M. S. degrees from Jiaozuo Institute and Technology, Henan Polytechnic University, Jiaozuo, China, in 1998 and 2005, respectively. He received the Ph.D. degree in School of Information and Electrical Engineering at China University of Mining and Technology, Xuzhou, China. His main research interests include the theory, application and control of linear motor.

As one of the research term, from 2007 to 2008, he was with ASM Pacific Technology Ltd., HongKong, as a Research Engineer. New, he is a teacher in School of Electrical Engineering and Automation, Henan Polytechnic University, china.

Mr. SI is a member of institute of linear electric machine and drives, Henan Province, China. In recent years, he participates in 8 provincial and 2 country research projects, published more than 30 academic papers.

Haichao FENG was born in China in 1983, and received the B.S. and M.S. degrees in electrical engineering and automation, control theory and control engineering from School of Electrical Engineering and Automation, Henan Polytechnic University, china

From 2007 to 2008, he was with ASM Pacific Technology Ltd., HongKong, as a Research Engineer. Now, he is a teacher in School of Electrical Engineering and Automation, Henan Polytechnic University, china.

Mr. FENG is a member of institute of linear electric machine and drives, Henan Province, China. In recent years, he participates in 5 provincial and 2 national research projects, published more than 8 academic papers.

Baoyu XU was born in Jiaozuo city, Henan Province, China in1963, and received the PH.D degree in mechanical design and manufacturing from College of Mechanical & Electrical Engineering, Central South University, China , in 2011. His research interests are stochastic vibration and dynamic behavior of mechanical systems.

Since 1996, He has been working in School of Mechanical and Power Engineering, Henan Polytechnic University, china mainly engaged in teaching and scientific research.

Dr. Xu is a member of institute of linear electric machine and drives, Henan Province, China. In recent years, he presided 2 provincial and one national research project, obtained two provincial academic rewards, and published more than 10 academic papers.